

Fabrication of Oxetane-Substituted Chitosan-Polyurethane Films with Excellent Anticorrosion and Self-Healing Performances

Chengcheng Ma^{1,2}, Jianguo Liu^{1,*}, Qi Wang², Wei Wang^{1,2,*}

¹ Shandong Key Laboratory of Oil & Gas Storage and Transportation Safety, China University of Petroleum (East China), Qingdao, 266580, China.

² School of Materials Science and Engineering, Ocean University of China, Qingdao, 266100, China.

*E-mail: wangwei8038@ouc.edu.cn, liujianguo@upc.edu.cn

Received: 17 July 2020 / Accepted: 3 September 2020 / Published: 30 September 2020

The oxetane-substituted chitosan-polyurethane (OXE-CHI-PUR) film was synthesized using a simple, fast, and low-cost process, which is attractive for its many applications in the fields of self-healing anticorrosion. In this work, the OXE-CHI-PUR films with outstanding anticorrosion and self-healing performances were incorporated in epoxy resin coatings. SEM confirmed that the diameter of the OXE-CHI-PUR network film was approximately 380 μm ($\pm 4 \mu\text{m}$). FT-IR measurement proved that successful synthesis of the OXE-CHI-PUR network film. It is visually observed through the confocal laser scanning microscope that the scratched OXE-CHI-PUR coating has a self-healing tendency with UV irradiation. The electrochemical impedance spectroscopy (EIS) experiments analyzed the self-healing performance of OXE-CHI-PUR coating. The results of EIS and 14 days' seawater immersion tests revealed that the coating containing OXE-CHI-PUR films showed high anticorrosion performance and exhibited self-healing capabilities due to the influence of light and heat.

Keywords: UV irradiation; Self-healing performance; Anticorrosion

1. INTRODUCTION

In recent years, due to the dual pressures of global energy and environmental protection, marine anti-corrosion has received more and more attention. [1, 2] Organic coatings have been widely used in the marine industry and marine structures to prevent corrosion of metals including steel, copper, magnesium alloys and aluminum alloys. [3] Self-healing materials have attracted great attention due to their ability to recover autonomously after suffering unnecessary external damage. [4-7] When the coating is broken due to mechanical shock, scratching or impact, the damaged area of the coating will accelerate metal corrosion. The self-healing method functionalizes the coating material to form a passive

barrier to prevent the passage of oxygen and water after mechanical damage. [8] Therefore, smart coatings are urgently needed to extend the life of damaged coatings.

Light-induced shape memory polymers (SMP) are smart materials that undergo large recoverable deformations when light energy is applied. Based on the shape memory mechanism of polymers, light-induced SMP includes photochemically-induced SMP and photothermal-induced SMP. Photothermal agents are commonly used to prepare photothermally induced SMP, such as carbon nanotubes [9, 10], reduced graphene oxide [11, 12] and conjugated polymers [13-15] can thermally guide SMP. Under light irradiation, the photothermal agent can absorb light energy and convert it into heat energy. Therefore, the temperature of these polymers can be raised above their glass transition temperature (T_g) or melting temperature (T_m) to cause molecular chain movement and entanglement to restore its original shape. Self-healing polymer materials can be produced by combining oxetane-substituted chitosan (OXE-CHI) and polyurethane (PUR) into a cross-linked network. [16] The choice of the components depends on their ability to serve specific functions. The isocyanate-polyol crosslinking reaction leads to the formation of PUR and/or polyurea (PUA), which provides ideal mechanical integrity and local network heterogeneity. The OXE-CHI macromonomer is incorporated into the PUR network as a cross-linking agent, which facilitates to cleave the constrained 4-membered ring (OXE) and external response sensitivity (CHI) required for self-healing [17].

In this paper, electrochemical techniques were used to study the mechanism of anticorrosion and evaluate the self-healing performance of OXE-CHI-PUR coatings. Fourier-transform infrared (FT-IR) spectroscopy was used to prove that successful synthesis of the OXE-CHI-PUR network film. Finally, the OXE-CHI-PUR coatings exhibited excellent self-healing anticorrosion properties.

2. EXPERIMENTAL

2.1 Materials

Chitosan (CHI, $M_n \approx 5 \times 10^5$), sodium hydroxide (NaOH), sodium chloride (NaCl), dimethyl sulfoxide (DMSO, 99.0%), methanol, and isopropanol were purchased from Sinopharm Chemical Reagent Co., Ltd. (Shanghai, China). Acetic acid (CH_3COOH , 99.5%), polyethylene glycol 200 (PEG-200), absolute ethyl alcohol and acetone were purchased from Shanghai Chemicals Co., Ltd, China. 3-(Chloromethyl)-3-methyloxetane (98.0%) was purchased from Macklin Biochemical Co., Ltd. (Shanghai, China). Dibutyltin dilaurate (DBTDL, 95%) was purchased from Aladdin Bio-Chem Technology Co., Ltd. (Shanghai, China). Tri-functional Hexamethylene diisocyanate (99.5% HDI) was purchased from Wanhua Chemical Group Co., Ltd. (Yantai, China). Ultrapure deionized water was used for all solution preparation. All the reagents were used without further purification.

Q235 steel was purchased from Shanghai BaoSteel. Epoxy resin (E20, epoxy equivalent 450 g/eq) was purchased from Xingchen Synthetic Material Co., Ltd. (Nantong, China). Polyamide curing agent (650, amine value 235~243 mgKOH/g) was purchased from Danbao resin Co., Ltd. (Zhenjiang, China).

2.2 Preparation of OXE-CHI-PUR

Firstly, 0.3 g of CHI was added to 50 mL 1mol/L NaOH solution, stirred for 12 h at 0 °C, and then frozen at -18 °C for 48 h. The solution was thawed and mixed with pre-chilled isopropanol and stirred for 1 h. The pre-cooled 3-(chloromethyl)-3-methyloxetane was added to the mixture, and then the solution was stirred at 80 °C for 12 h. The product was filtered and washed with methanol several times until it became neutral, and then dried at 60 °C for 12 h. To polymerize oxetane-substituted chitosan (OXE-CHI), 1 : 1 mole of OXE-CHI was dispersed in DMSO (in the presence of 2×10^{-5} moles of DBTDL) and acetic acid (pH=6.8) solutions, and then exposed to ultraviolet radiation for 1 hour. The polymerized OXE-CHI was separated by washing with methanol. To prepare OXE-CHI-PUR networks, the OXE-CHI macromonomer was dispersed in DMSO by sonicating the solution at 25 °C for 12 h, and then continuously stirring at 80 °C for 48 h. The OXE-CHI-PUR films were prepared by reacting HDI with dispersed OXE-CHI and PEG using overhead agitation at 500 rpm with a small four-blade polytetrafluoroethylene (PTFE) impeller in a 50 mL three-neck reaction flask at 25 °C for 10 min under N₂ atmosphere. By adjusting stoichiometric ratios of —NCO, —OH, and —NH₂ reactive groups, a series of PUR networks were prepared. On the PTFE substrate, the OXE-CHI-PUR film of approximately 380 μm (± 4 μm) was fabricated for 12 h under the conditions of 30 °C and 15% relative humidity (RH), and then fabricated in a vacuum oven at 80 °C for 48 h. The whole process of synthesizing OXE-CHI-PUR film is shown in Figure 1.

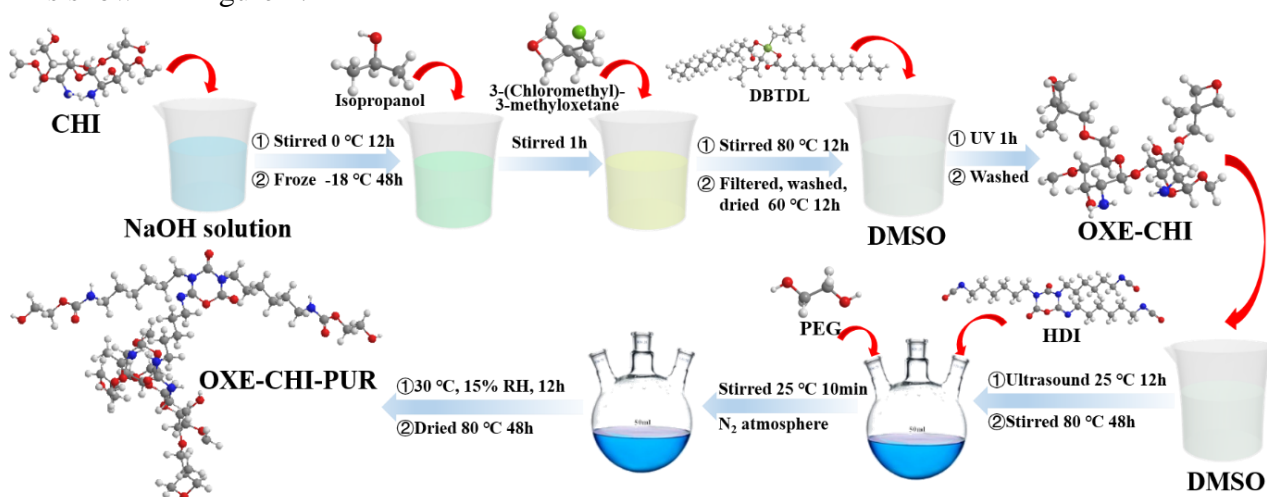


Figure 1. Schematic illustration of the OXE-CHI-PUR films synthesis.

2.3 Preparation of working electrodes

The working electrodes were prepared using Q235 steel with an exposed area (1 cm^2) polished by 360, 800 and 1000# sand papers, respectively. Firstly, the steel blocks were deoiled in the 0.5 M NaOH aqueous solution and rinsed with absolute ethyl alcohol (95%) and deionized water. After washing, they were quickly dried to avoid corrosion. Then, the steel bars were respectively welded with a copper line and embedded in epoxy resin molds. The liquid epoxy resin was solidified by adding 10 wt.% polyamide curing agent. When the epoxy resin became hard enough, the working electrode combined with hardened epoxy resin was carefully lifted back from the mold. Finally, the side surface

and an end surface of the bars were sealed to prevent corrosion. A bare end surface was reserved for the following electrochemical tests.

2.4 Scanning electron microscope (SEM)

The morphology and size of the fabricated samples were certified with scanning electron microscopy (SEM, Phenom ProX, China).

2.5 Fourier transform infrared spectroscopy (FT-IR)

Infrared spectral analysis was used to evaluate the synthetic degree of the self-healing agent. The component analysis of different samples was determined by the Fourier transform infrared spectroscopy (FT-IR) IS-50 spectrometer (Nicolet, America) with KBr discs. A drop of the colloidal solution was dripped between two pieces of KBr to form a liquid film for testing.

2.6 Electrochemical measurements

A three-electrode system was used in this study. The exposed area of working electrode (with specimen) was 1 cm², and the electrolyte was 3.5 wt.% NaCl solution. Firstly, a steady open circuit potential (OCP) was obtained through immersing specimen in the electrolyte for about 30 min. Then the electrochemical impedance spectra (EIS) tests were scanned with a frequency range from 100 kHz to 0.01 Hz.

2.7 Confocal laser scanning microscope (CLSM)

The scratch morphology and maximum pit depth on the scratched OXE-CHI-PUR coating were examined under a CLSM (Model VK-X250 K, Keyence, Osaka, Japan) after 1 day, 3 days of UV irradiation, and 7 days without UV irradiation respectively.

2.8 Infrared thermal imaging camera

The FOTRIC 324 infrared thermal imaging camera was purchased from Beijing Stacent Technology Co., Ltd. The scratched OXE-CHI-PUR coating before and after 3 day of UV irradiation was observed under a FOTRIC 324 infrared thermal imaging camera respectively.

3 RESULTS

3.1 Morphology and structural characterization

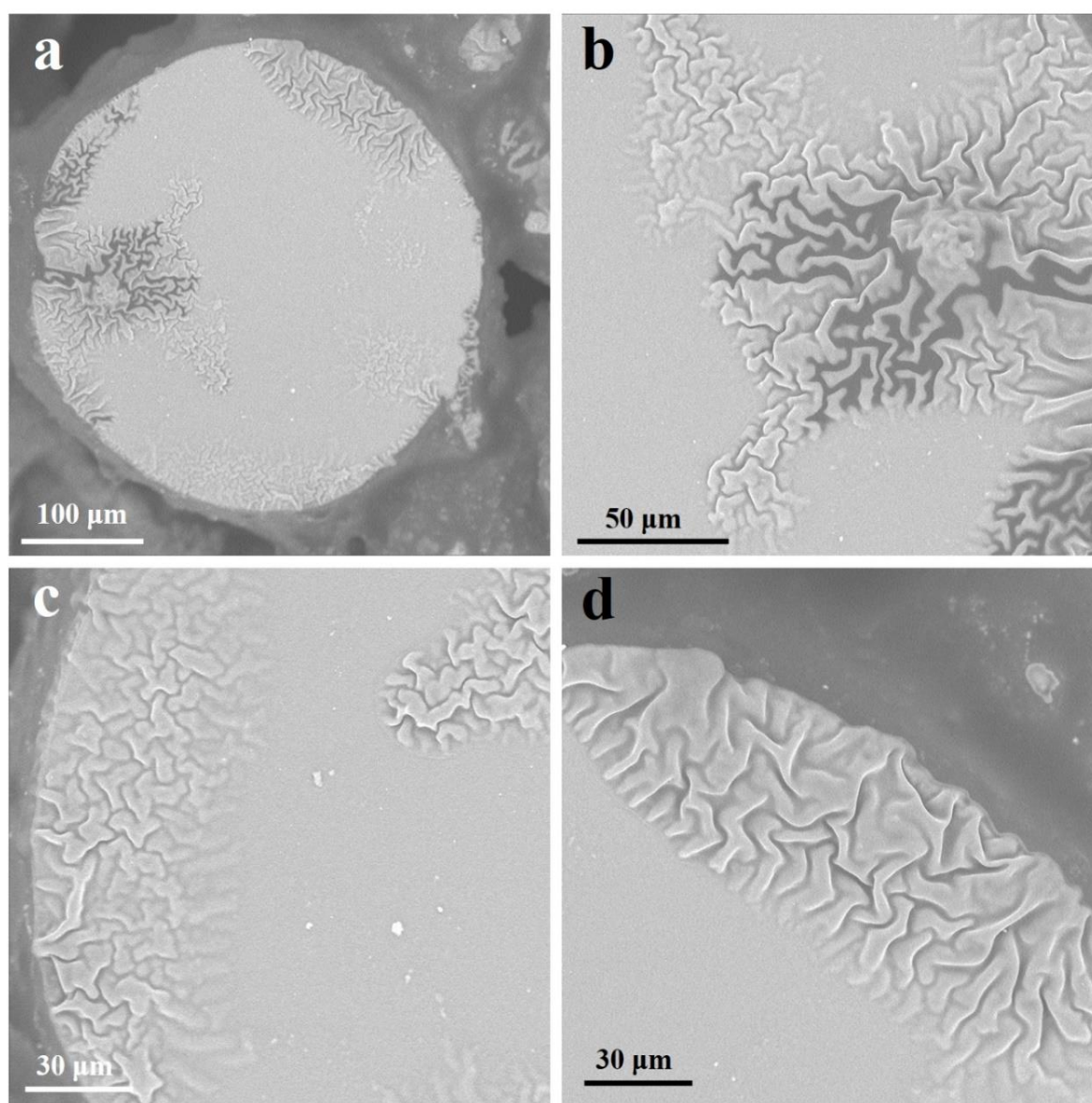


Figure 2. SEM images of OXE-CHI-PUR films.

It can be seen from Figure 2 that the film-like substance is a cross-linked OXE-CHI-PUR network film, whose diameter is approximately 380 μm (± 4 μm). When OXE-CHI-PUR network film is damaged, chemical bonds break to form free radicals, and the network reorganization and self-healing process begins at the lowest point of the scratch with the highest surface energy.

3.2 FT-IR analysis

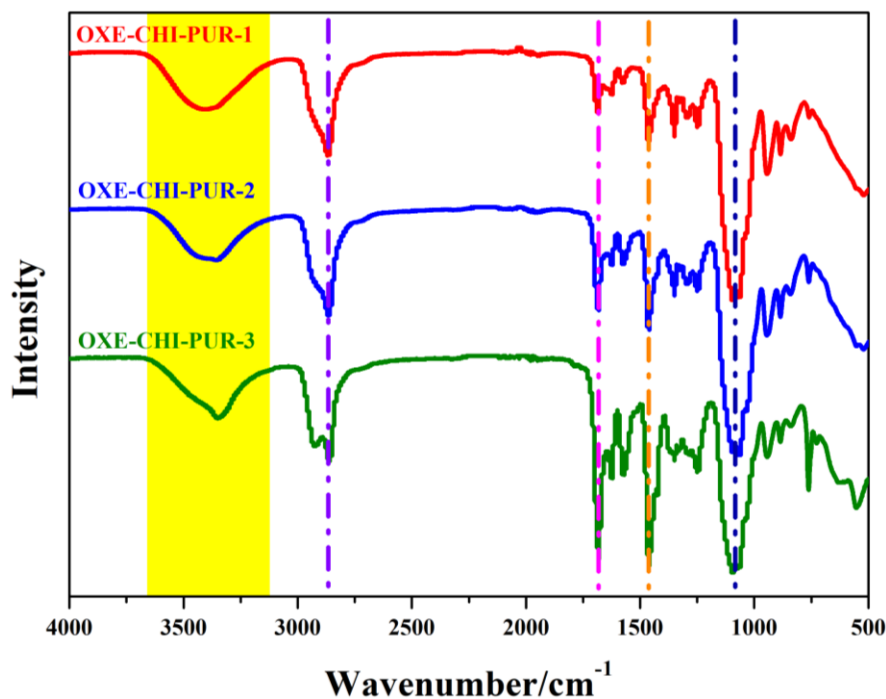


Figure 3. FT-IR spectrogram of OXE-CHI-PUR.

Figure 3 shows the FT-IR spectra of OXE-CHI-PUR-1 (translucent and sticky sample), OXE-CHI-PUR-2 (opaque and sticky sample) and OXE-CHI-PUR-3 (transparent and hard sample). For all samples, the broad vibration shrinkage peaks $3600\sim 3200\text{ cm}^{-1}$ corresponds to the stretching vibration of $-\text{OH}$ of CHI and $-\text{NH}$ in the polymer, and the vibration shrinkage peak 2867 cm^{-1} corresponds to the stretching vibration of $-\text{CH}_2$ in the polymer. In addition, the double peaks at 1684 cm^{-1} and 1634 cm^{-1} are assigned to the composite peak of $-\text{C}=\text{O}$ stretching vibration of $-\text{NHC}=\text{O}$ group in the polymer and $-\text{C}=\text{N}$ stretching vibration in HDI, respectively. The peak at $1484\sim 1414\text{ cm}^{-1}$ corresponds to the deformation vibration peak of $-\text{CH}_2$ or $-\text{CH}_3$ in the polymer. The peak at 1083 cm^{-1} represents the stretching vibration peak of chitosan, oxetane, and the ether bond between them [18]. In Figure 3, the composite peaks of $-\text{C}=\text{O}$ stretching vibration of $-\text{NHC}=\text{O}$ group and $-\text{C}=\text{N}$ stretching vibration in HDI at 1684 cm^{-1} and 1634 cm^{-1} peaks in OXE-CHI-PUR-3 are higher than those of OXE-CHI-PUR-1 and OXE-CHI-PUR-2, and these three products have different forms. This may be a polyurethane that has not completely reacted with the OXE-CHI precursor, because during the reaction, a part of HDI was observed to be incompletely mixed with the reaction solution in a phase-separated state. It may also be partly due to the influence of the reaction medium DMSO, because OXE-CHI-PUR-1 and OXE-CHI-PUR-2 are in a viscous state, and OXE-CHI-PUR-3 is a hard and transparent dry product, which may be interfered by the reaction medium DMSO. In the spectrum, there is no urea group characteristic peak of HDI at 2260 cm^{-1} , because it reacts with the amino group of chitosan to generate urea group of self-healing agent.

3.3 Anticorrosion and self-healing performances of OXE-CHI-PUR coating

In order to quantitatively evaluate the corrosion resistance of the scratched OXE-CHI-PUR coating after immersion for 1, 2, 3, 4, 6, 8, 10, 12, and 14 days, the EIS measurement was performed in 3.5 wt.% NaCl solution for different soaking times. EIS measurements could effectively monitor the self-healing process [19]. The total resistance combination of the Bode plot in EIS effectively showed the protective properties of the coating for Q235 steel [20].

Previous literature [21] pointed out that the impedance in the high frequency region represents the impedance of the interface layer, and the impedance in the low frequency region represents the shielding ability of the coating against the corrosive medium. The fitted data in Table 1 shows that the impedance of scratched OXE-CHI-PUR coating is the highest for 6 days of immersion; with the extend of immersion time, the impedance of scratched OXE-CHI-PUR coating shows a trend of increasing first and then decreasing. Figure 4a illustrates the self-healing process that occurred during the first 6 days, which directly prevented the solution from penetrating to the bottom of the gap, because the inherent elasticity of the epoxy caused the two side walls of the scratch gap to contact each other. In addition, some residual OXE-CHI-PUR materials also reduced the penetration rate of NaCl solution within 6 days after scratching. The Bode diagram in Figure 4b reveals two time constants: one is the time constant in the mid-frequency range caused by the self-healing coating, and the other is the time constant in the low-frequency range attributable to the response of processes occurring at the coating/substrate interface [22]. The upward trend of the phase angle curves in the mid-frequency range (Figure 4c) shows that the resistance of the OXE-CHI-PUR coating has been enhanced through the self-healing process. Due to the self-healing coating protection function, the capacitance response in the mid-frequency range and the corresponding resistance response in the low-frequency range.

In general, the impedance modulus at 0.01 Hz ($|Z|_{0.01\text{Hz}}$) can be used to indicate the ability of OXE-CHI-PUR coating to suppress the current running between the anode and the cathode [23]. Normally, the larger the $|Z|_{0.01\text{Hz}}$ value, the better the corrosion resistance. At the same time, in a wide frequency range, the phase angle value of a perfect coating without defects should be -90° . As the corrosive medium slowly diffuses into the metal/coating interface, the phase angle value at a given frequency will decrease due to the capacitance characteristics of the coating. Thus, the changes in phase angle diagram at a given frequency are usually used to reflect the corrosion resistance of the coating. Similarly, the peaks centered at different frequencies in the Bode modulus or phase angle diagram can reflect different time constants. Generally, the time constant in the low frequency range should be attributed to the corrosive process at the metal/coating interface, while that in the high frequency range should attributed to the coating.

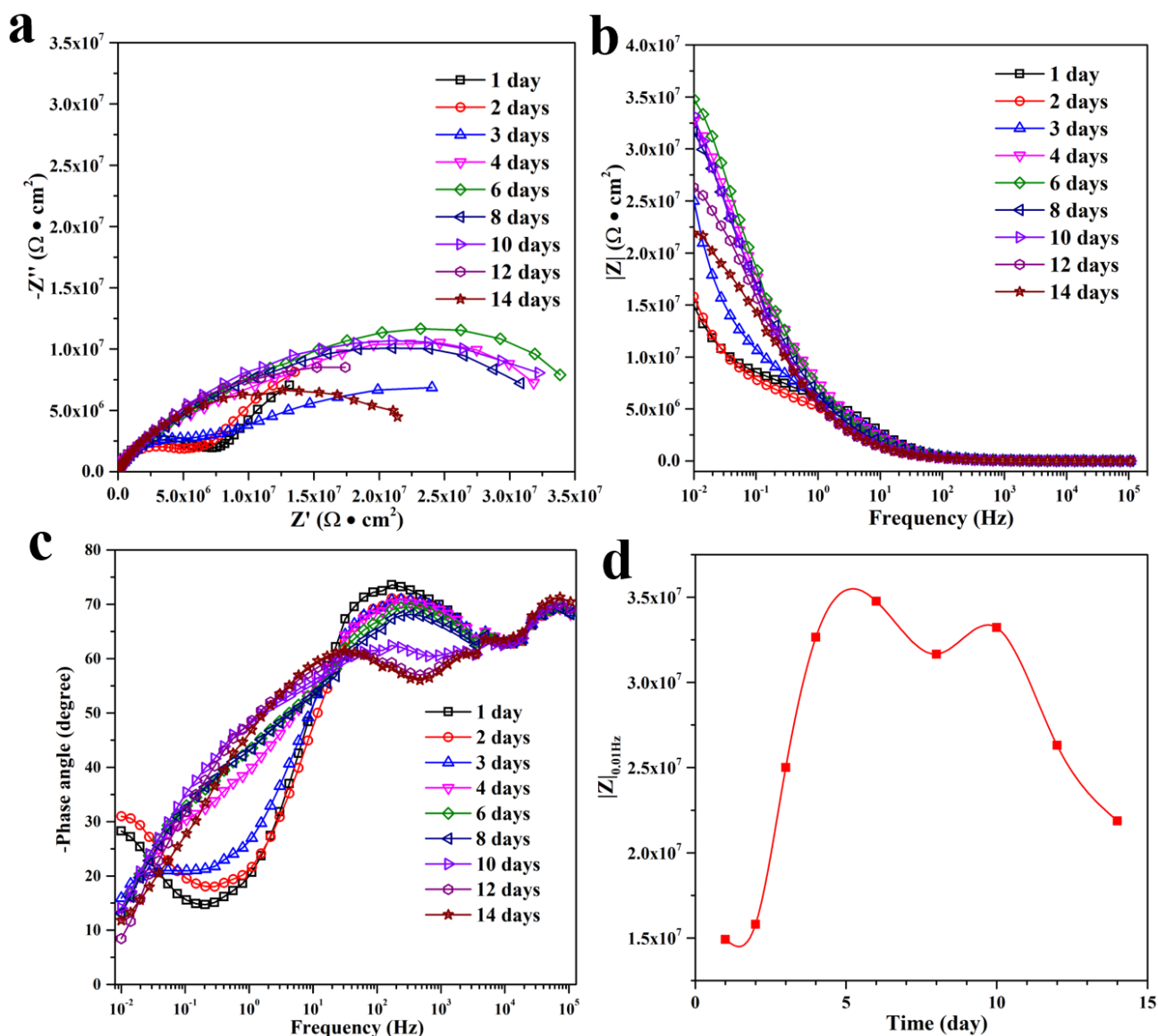


Figure 4. Nyquist plot (a), module plots of impedance (b), phase plots of impedance (c) of scratched OXE-CHI-PUR coatings after 1, 2, 3, 4, 6, 8, 10, 12, and 14 days immersion. $|Z|_{0.01\text{Hz}}$ plots of scratched OXE-CHI-PUR coatings after 14 days immersion (d).

As for the scratched OXE-CHI-PUR coatings, after 14 days of immersion, the $|Z|_{0.01\text{Hz}}$ value is still higher than $2 \times 10^7 \Omega \text{ cm}^2$ (Figure 4d). Meanwhile, in the Bode angle diagram (Figure 4c), there is only one time constant with the phase angle peak appearing at about -70° , which indicates that the capacitance properties of the composite coating are maintained. After 6 days of immersion, the $|Z|_{0.01\text{Hz}}$ value of the scratched OXE-CHI-PUR coating is approximately $3.5 \times 10^7 \Omega \text{ cm}^2$ (Figure 4d). At the same time, the second time constant that appears in the low frequency range is showed in the Bode angle graph. This indicates that corrosion initially occurs at the coating/metal interface. Interestingly, the $|Z|_{0.01\text{Hz}}$ values of the scratched OXE-CHI-PUR coating rebounded to $2.19 \times 10^7 \Omega \text{ cm}^2$ with the extension of the immersion time (i.e., 14 days). Moreover, in the Bode phase angle diagrams, one time constant and peak phase angle at about -70° reappeared. This shows that due to the self-healing performances of OXE-

CHI-PUR coating, the corrosion at the coating/metal interface has been prevented and the corrosion resistance is enhanced.

Table 1. EIS parameters of scratched OXE-CHI-PUR coatings obtained by fitting the measured impedance data.

Immersion time (days)	R_c ($\Omega \text{ cm}^2$)	CPE_c		C_c (F/cm^2)	R_{ct} ($\Omega \text{ cm}^2$)	CPE_{dl}		C_{dl} (F/cm^2)
		Y_c ($\text{F cm}^{-2} \text{ S}^{n-1}$)	n_c			Y_{dl} ($\text{F cm}^{-2} \text{ S}^{n-1}$)	n_{dl}	
1	7.51×10^6	1.21×10^{-8}	0.79	3.18×10^{-8}	3.43×10^7	6.42×10^{-7}	0.70	2.56×10^{-6}
2	6.04×10^6	1.41×10^{-8}	0.78	3.88×10^{-8}	4.44×10^7	4.46×10^{-7}	0.64	2.34×10^{-6}
3	5.93×10^4	8.55×10^{-8}	0.19	3.56×10^{-6}	4.88×10^{16}	1.17×10^{-8}	0.80	2.94×10^{-8}
4	9.31×10^6	1.62×10^{-8}	0.77	3.43×10^{-8}	3.17×10^7	7.30×10^{-8}	0.63	2.44×10^{-7}
6	7.59×10^6	1.86×10^{-8}	0.76	4.41×10^{-8}	3.95×10^7	5.48×10^{-8}	0.57	2.57×10^{-7}
8	6.59×10^6	2.11×10^{-8}	0.75	4.76×10^{-8}	3.36×10^7	5.56×10^{-8}	0.58	2.18×10^{-7}
10	3.02×10^4	1.00×10^{-8}	0.80	2.05×10^{-8}	4.17×10^7	4.41×10^{-8}	0.56	2.14×10^{-7}
12	3.02×10^4	7.75×10^{-9}	0.82	1.78×10^{-8}	2.89×10^7	4.20×10^{-8}	0.61	2.53×10^{-7}
14	6.34×10^4	7.97×10^{-9}	0.82	1.20×10^{-8}	2.32×10^7	3.99×10^{-8}	0.62	9.40×10^{-8}

In addition, the equivalent circuit (Figure 5) was used to fit the EIS data of the scratched OXE-CHI-PUR coating during the self-healing process. R_s is the solution resistance of 3.5 wt.% NaCl solution. R_c represent the coating resistance and Q_c represent the capacitance of the scratched OXE-CHI-PUR coating. R_{ct} represent the metal charge transfer resistance and Q_{dl} represent double layer capacitance. C_c and C_{dl} represent the capacitance of the scratched OXE-CHI-PUR coating and the metal double layer capacitance during the pre-self-healing process. For the capacitive loops, the coefficients n_c and n_{dl} represent the depressed characteristics in the Nyquist diagram. The corresponding capacitance value is calculated by Equation 1: [24, 25]

$$C = Y(\omega_{\max})^{n-1} \quad (1)$$

where ω_{\max} is the frequency at which the imaginary part of the impedance shows the maximum value, and Y and n are the magnitude and exponential term of the CPE, respectively.

The coating resistances R_c of the scratched OXE-CHI-PUR coating (fitting result of experimental EIS) are plotted in Figure 6a. During the immersion process, the values of R_c has the same trend of $|Z|_{0.01\text{Hz}}$ values (Figure 4d). According to the fitting results of the first 3 days in Table 1, the decreasing trend of R_c value (from $7.51 \text{ M}\Omega \text{ cm}^2$ to $5.93 \times 10^4 \Omega \text{ cm}^2$) indicates that during the pre-self-healing process, the solution slowly penetrated to the bottom of the crevice. However, the increasing tendency of the R_c value (from $5.93 \times 10^4 \Omega \text{ cm}^2$ to $9.31 \text{ M}\Omega \text{ cm}^2$) indicates that the self-healing process enhanced the barrier of the scratches in OXE-CHI-PUR coating.

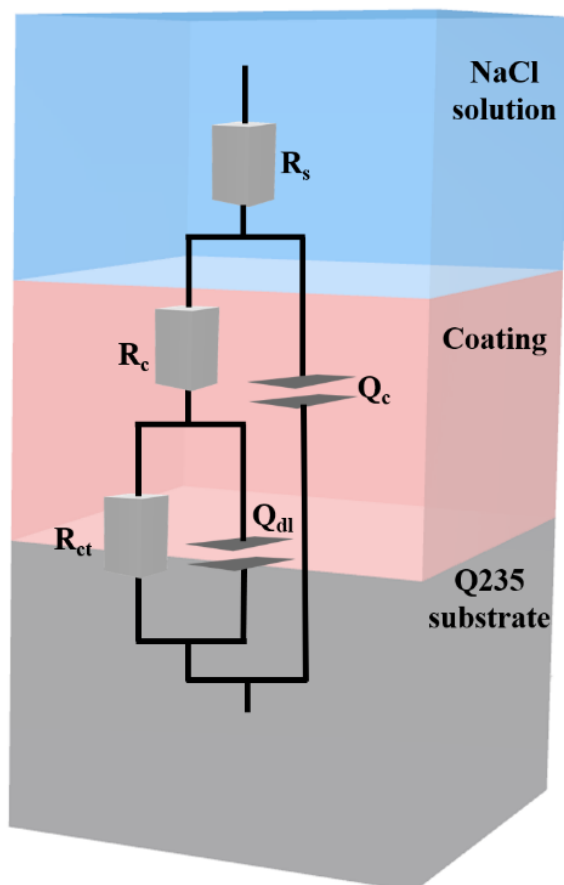


Figure 5. Equivalent circuit models used to fit the experiment impedance data of scratched OXE-CHI-PUR coatings in 3.5 wt.% NaCl solution.

After 6 days of immersion, the R_c value gradually decreased, indicating that the barrier properties of the OXE-CHI-PUR coating gradually decreased due to penetration. The constant phase elements of the coating Q_c are showed in Table 1. Before 3 days, the Q_c values gradually increased (from 0.0318 to $3.56 \mu\text{F cm}^{-2}$). However, during the 14-day immersion period, the Q_c values gradually decreased (from 3.56 to $0.012 \mu\text{F cm}^{-2}$) with slight fluctuations. The reciprocals of charge-transfer resistance ($1/R_{ct}$) and the constant phase element of double layer capacitance (Q_{dl}) are showed in Table 1. The $1/R_{ct}$ values are used to indicate the corrosion rate of steel in different environments [26]. The lower the $1/R_{ct}$ value of the coating, the greater its corrosion resistance [27]. In addition, during the self-healing process, the Q_{dl} value dropped sharply, indicating that the self-healing process was in progress.

Figure 6 shows 3D morphologies and maximum pit depths on the scratched OXE-CHI-PUR coating obtained from CLSM. The results show that the maximum pit depth of the scratched OXE-CHI-PUR coating is $153.49 \mu\text{m}$ after being irradiated with ultraviolet light for 1 day. But after 3 days of UV irradiation, the maximum pit depth was $86.37 \mu\text{m}$. The results prove that the OXE-CHI-PUR coating has UV-cured self-healing performance. However, after 7 days without UV irradiation, its maximum pit depth is $284.29 \mu\text{m}$, which means that without UV exposure, the scratched OXE-CHI-PUR coating tends to fail.

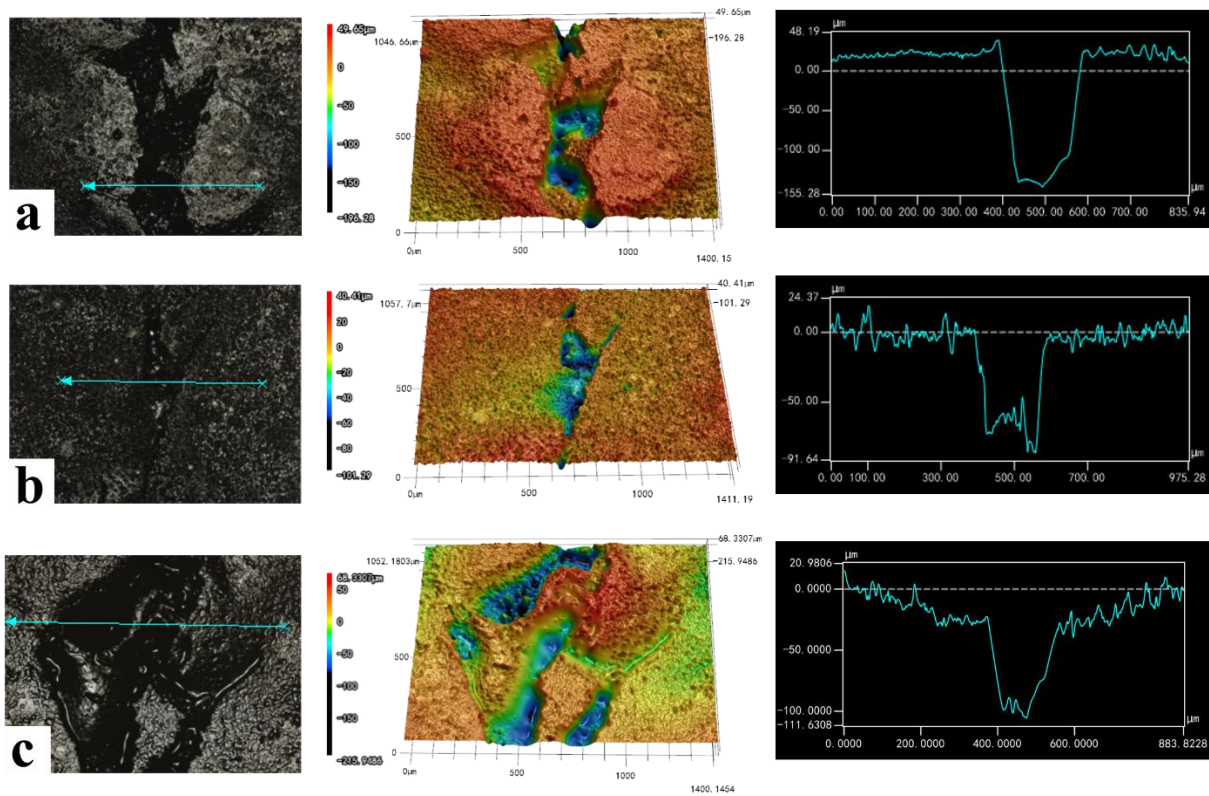


Figure 6. 3D Pitting morphologies and maximum scratch depths measured under CLSM on the scratched OXE-CHI-PUR coating after 1 day (a), 3 days (b) of UV irradiation and 7 days without UV irradiation, respectively.

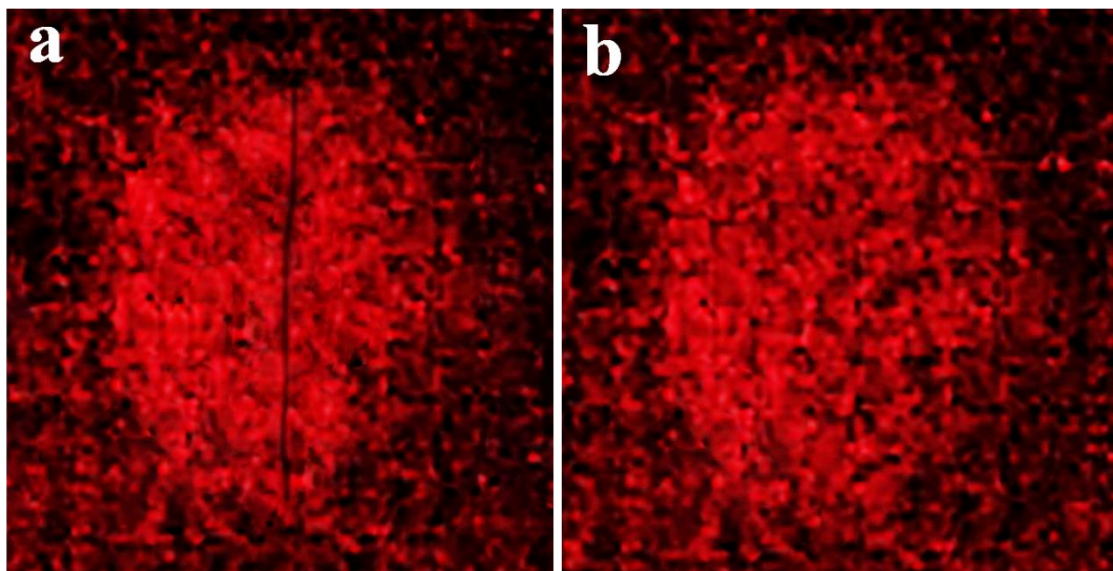


Figure 7. The scratched OXE-CHI-PUR before (a) and after 3 day of UV irradiation (b).

Figure 7 shows the scratched OXE-CHI-PUR coating before (Figure 7a) and after (Figure 7b) 3 day of UV irradiation obtained from a FOTRIC 324 infrared thermal imaging camera respectively. It can be seen from the Figure 8 that after 3 days of UV irradiation, the scratched OXE-CHI-PUR coating

gradually self-healed, which corresponds to the previous CLSM results. The above experimental results prove that UV irradiation can stimulate the self-healing of the scratch of OXE-CHI-PUR coating, which means that the OXE-CHI-PUR coating has UV-responsive self-healing performance.

The corrosion resistance is attributed to the self-healing ability of the OXE-CHI-PUR coating. The mechanism of self-repair and corrosion protection is shown in Figure 8. Firstly, the mechanical damage caused the coating to crack, and the ions (Na^+ and Cl^-) in the water in the crack directly contacted the mild steel to cause corrosion. However, under the effect of light and heat, the coating caused the network composed of reformed urethane and ether bonds to self-healing. The OXE-CHI-PUR film can act as a barrier to the diffusion of electrolytes and aggressive ions, thereby protecting the mild steel.

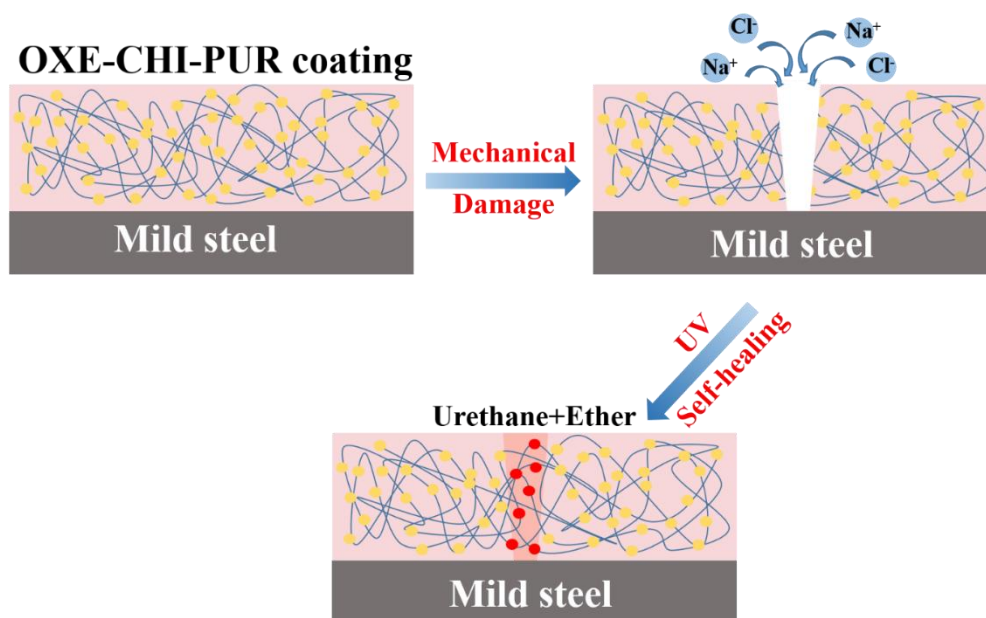


Figure 8. The mechanism of self-healing and corrosion protection of the OXE-CHI-PUR coating.

4. CONCLUSIONS

In this study, SEM and FT-IR spectroscopy were used to prove the successful synthesis of OXE-CHI-PUR. Electrochemical techniques were used to understand the mechanism of anticorrosion and evaluate the self-healing performance of OXE-CHI-PUR coating. The CLSM results proved that the OXE-CHI-PUR coating has UV-cured self-healing performance. Finally, we conclude that the OXE-CHI-PUR coating has excellent UV-cured self-healing properties and has the potential to be applied in practice in the future.

ACKNOWLEDGEMENTS

This work was supported by the Fundamental Research Funds for the Central Universities (19CX05007A, 201912032, 201965009) and the Opening fund of Shandong Key Laboratory of Oil & Gas Storage and Transportation Safety.

CONFLICT OF INTEREST

The authors declare no financial or commercial conflict of interest.

References

1. H. Chen and D. Kong, *J. Alloy. Compd.*, 771 (2019) 584-594.
2. M. Cao, L. Liu, Z. Yu, L. Fan, Y. Li and F. Wang, *J. Mater. Sci. Technol.*, 35 (2019) 651-659.
3. S. Chen, B. Zhu, X. Liang, *Int. J. Electrochem. Sci.*, 15 (2020) 1-15.
4. G. Xi, X. Zhao, S. Wang, J. Yang, J. Sun, Z. An, Y. Li and X. Qu. *Int. J. Electrochem. Sci.*, 15 (2020) 361-370.
5. W. Wang, W. Li, W. Fan, X. Zhang, L. Song, C. Xiong, X. Gao and X. Liu, *Chem. Eng. J.*, 332 (2018) 658-670.
6. X. Ji, W. Wang, W. Li, X. Zhao, A. Liu, X. Wang, X. Zhang, W. Fan, Y. Wang, Z. Lu, S. Liu and H. Shi, *J. Taiwan Inst. Chem. E.*, 104 (2019) 227-239.
7. C. E. Diesendruck, N. R. Sottos, J. S. Moore and S. R. White, *Angew. Chem. Int. Ed. Engl.*, 54 (2015) 10428-10447.
8. W. Fan, Y. Zhang, W. Li, W. Wang, X. Zhao and L. Song, *Chem. Eng. J.*, 368 (2019) 1033-1044.
9. W. Wang, H. Wang, J. Zhao, X. Wang, C. Xiong, L. Song, R. Ding, P. Han and W. Li, *Chem. Eng. J.*, 361 (2019) 792-804.
10. B. Qian, Z. Song, L. Hao, W. Wang and D. Kong, *J. Electrochem. Soc.*, 164 (2017) C54-C60.
11. X. Cui, J. Chen, Y. Zhu and W. Jiang, *Chem. Eng. J.*, 382 (2020) 122823.
12. S. S. Mahapatra, S. K. Yadav, B. H. Lee and J. W. Cho, *Polymer*, 160 (2019) 204-209.
13. Y. Bai, J. Zhang, D. Wen, P. Gong and X. Chen, *Compos. Sci. Technol.*, 170 (2019) 101-108.
14. V. D. Punetha, Y.-M. Ha, Y.-O. Kim, Y. C. Jung and J. W. Cho, *Polymer*, 181 (2019) 121791.
15. G. Qin and J. Qiu, *Chem. Eng. J.*, 359 (2019) 652-661.
16. Y. Bai, J. Zhang and X. Chen, *ACS Appl. Mater. Inter.*, 10 (2018) 14017-14025.
17. S. Yang, X. Du, Z. Du, M. Zhou, X. Cheng, H. Wang and B. Yan, *Polymer*, 190 (2020) 122219.
18. B. Ghosh and M. W. Urban, *Science*, 323 (2009) 1458-1460.
19. B. Ghosh, K. V. Chellappan and M. W. Urban, *J. Mater. Chem.*, 21 (2011) 14473-14486.
20. R. Li, J. Chen, T. Zhou and J. Pei, *Constr. Build. Mater.*, 105 (2016) 336-342.
21. W. Wang, L. Xu, X. Li, Y. Yang and E. An, *Corros. Sci.*, 80 (2014) 528-535.
22. G. W. Walter, *Corros. Sci.*, 26 (1986) 681-703.
23. W. Trabelsi, P. Cecilio, M. G. S. Ferreira and M. F. Montemor, *Prog. Org. Coat.*, 54 (2005) 276-284.
24. I. A. Kartsonakis, A. C. Balaskas, E. P. Koumoulos, C. A. Charitidis and G. Kordas, *Corros. Sci.*, 65 (2012) 481-493.
25. N. Sarkar, G. Sahoo, R. Das, G. Prusty, D. Sahu and S. K. Swain, *Ind. Eng. Chem. Res.*, 55 (2016) 2921-2931.
26. C. H. Hsu and F. Mansfeld, *Corrosion*, 57 (2001) 747-748.
27. X. Gao, S. Liu, H. Lu, F. Gao and H. Ma, *Ind. Eng. Chem. Res.*, 54 (2015) 1941-1952.
28. W. J. Lorenz and F. Mansfeld, *Corros. Sci.*, 21 (1981) 647-672.
29. Y. Shao, H. Huang, T. Zhang, G. Meng and F. Wang, *Corros. Sci.*, 51 (2009) 2906-2915.